 CMES, vol.14, no.1, pp.45-56, 2006

# A Parallel Multi-block Method for the Unsteady Vorticity-velocity Equations

**A. Grimaldi**[1] **, G. Pascazio**[2] **, M. Napolitano**[3]

**Abstract:** This paper provides a numerical method for solving two- and three-dimensional unsteady incompressible flows. The vorticity-velocity formulation of the Navier–Stokes equations is considered, employing the vorticity transport equation and a second-order Poisson equation for the velocity. Second-order-accurate centred finite differences on a staggered grid are used for the space discretization. The vorticity equation is discretized in time using a fully implicit three-level scheme. At each physical time level, a dual-time stepping technique is used to solve the coupled system of non linear algebraic equations by various efficient relaxation schemes. Steady flows are computed by dropping the physical time derivative and converging the pseudo-time-dependent problem. A domain decomposition of the physical space is also employed: the multi-block algorithm allows one to handle multiply-connected domains and complex configurations and, more importantly, to solve each grid-block on a single processor of a parallel platform. The accuracy and efficiency of the proposed methodology is demonstrated by solving well known two-dimensional flow problems. Then, the steady and unsteady flows inside a cubic cavity are considered and the numerical results are compared with experimental and numerical data.

## 1 Introduction

Vorticity plays a fundamental role in the physics of vortex dominated flows, its dynamics being the primary tool to understand the time evolution of vortical structures. Therefore, in the numerical solution of the time-dependent incompressible Navier–Stokes equations it is convenient to use vorticity as one of the dependent variables. In order to be able to solve two- and three-dimensional flows, the velocity vector is used in this work as the second dependent variable, as originally proposed by Fasel (1976). In particular, the vorticity-velocity formulation has the remarkable property that, when using a non-inertial reference frame, *non-inertial effects enter into the solution of the problem through the implementation of initial and boundary conditions* (Speziale, 1987), the governing equations remaining formally unchanged. In addition to such an advantage, it has been recently recognized that the vorticity-velocity formulation can be a viable approach for large eddy simulations (Winckelmans, Lund, Carati, and Wray, 1996). Following such a suggestion, LES have been performed using both particle-based Lagrangian formulations (Mansfield, Knio, and Menevau, 1998) and Eulerian-based formulations (Tenaud, Pellerin, Dulieu, and Phuoc, 2005).

The authors have developed numerical methods for solving the vorticity-velocity formulation of the Navier–Stokes equations in two-dimensional general curvilinear coordinates for both steady (Pascazio and Napolitano, 1996) and unsteady problems (De Palma, Pascazio, and Napolitano, 2001). The scalar vorticity transport equation is coupled with a second-order equation for the velocity vector, obtained by combining the vorticity definition and the incompressibility condition. The equations are discretized in space by a staggered-grid second-order-accurate finite-volume method and the problem is closed by computing the vorticity at the boundary by means of its definition. For steady flows, the three equations are solved by an alternating direction line-Gauss–Seidel relaxation scheme, using a false-transient approach (Pascazio and Napolitano, 1996). For unsteady flows, the vorticity transport equation is discretized in time by means of an implicit three-level scheme and the solution at each time level is obtained through a dual time-stepping technique (Pascazio, Grimaldi, and Napolitano, 2003): a multigrid line-Gauss–Seidel relaxation scheme is applied to solve the nonlinear coupled vorticity-velocity system at each physical time level, the vorticity time-derivative being a source term in the vorticity transport equation.

[1] DIMeG & CEMeC, Politecnico di Bari, via Re David 200, 70125 Bari, Italy, e-mail: an.grimaldi@poliba.it.
[2] DIMeG & CEMeC, Politecnico di Bari, via Re David 200, 70125 Bari, Italy, e-mail: pascazio@poliba.it.
[3] DIMeG & CEMeC, Politecnico di Bari, via Re David 200, 70125 Bari, Italy, e-mail: napolita@poliba.it.

The aim of the present paper is to reduce the CPU time required by such a methodology either to reach the steady-state solution or to converge at each time level in unsteady computations, as well as to extend it to the solution of three-dimensional steady and unsteady problems. Therefore, more efficient relaxation schemes have been considered and a domain decomposition of the physical space has been employed in conjunction with a parallel multi-block algorithm.

In the following, the governing equations are presented and the numerical method is described; then, two- and three-dimensional steady and unsteady flows are computed to validate the numerical method and its multi-block implementation.

## 2 Governing equations

The non-dimensional incompressible Navier–Stokes equations read:

$$\frac{\partial \vec{u}}{\partial t} + \vec{\nabla}\left(\frac{u}{2}\right) - \vec{u}\times\vec{\omega} = -\vec{\nabla}p - \frac{1}{Re}\vec{\nabla}\times\vec{\omega}, \tag{1}$$

$$\vec{\nabla}\cdot\vec{u} = 0, \tag{2}$$

where $\partial$ is the partial derivative operator, $t$ is the time, $\vec{u}$ is the velocity vector, $p$ is the pressure, $Re$ is the Reynolds number, and $\vec{\omega}$ is the vorticity vector,

$$\vec{\omega} = \vec{\nabla}\times\vec{u}. \tag{3}$$

The vorticity transport equation is obtained by taking the *curl* of equation (1), to give

$$\frac{\partial \vec{\omega}}{\partial t} - \vec{\nabla}\times(\vec{u}\times\vec{\omega}) = -\frac{1}{Re}\vec{\nabla}\times\vec{\nabla}\times\vec{\omega}. \tag{4}$$

In equation (4), the right hand side is simplified using the following vector identity,

$$\vec{\nabla}\times\vec{\nabla}\times\vec{\omega} = \vec{\nabla}(\vec{\nabla}\cdot\vec{\omega}) - \nabla^2\vec{\omega}, \tag{5}$$

together with the divergence-free condition for the vorticity vector,

$$\vec{\nabla}\cdot\vec{\omega} = 0, \tag{6}$$

to give:

$$\frac{\partial \vec{\omega}}{\partial t} - \vec{\nabla}\times(\vec{u}\times\vec{\omega}) = \frac{1}{Re}\nabla^2\vec{\omega}. \tag{7}$$

Furthermore, in the numerical method, it is convenient to use also the non conservative form of the nonlinear advection term, which is obtained from the following vector identity

$$\begin{aligned}\vec{\nabla}\times(\vec{u}\times\vec{\omega}) &= \vec{u}(\vec{\nabla}\cdot\vec{\omega}) + (\vec{\omega}\cdot\vec{\nabla})\vec{u} \\ &- \vec{\omega}(\vec{\nabla}\cdot\vec{u}) - (\vec{u}\cdot\vec{\nabla})\vec{\omega}\end{aligned} \tag{8}$$

together with equations (2) and (6). The resulting *non conservative* vorticity transport equation reads:

$$\frac{\partial \vec{\omega}}{\partial t} + (\vec{u}\cdot\vec{\nabla})\vec{\omega} - (\vec{\omega}\cdot\vec{\nabla})\vec{u} = \frac{1}{Re}\nabla^2\vec{\omega}. \tag{9}$$

In order to solve the kinematic problem, it is convenient to obtain a second-order elliptic PDE for the velocity vector in place of the two first-order equations, (2) and (3), so as to use standard relaxation methods. Taking the *curl* of the vorticity definition, equation (3), and using the vector identity,

$$\vec{\nabla}\times\vec{\nabla}\times\vec{u} = \vec{\nabla}(\vec{\nabla}\cdot\vec{u}) - \nabla^2\vec{u},$$

together with the incompressibility condition, one obtains:

$$\nabla^2\vec{u} = -\vec{\nabla}\times\vec{\omega}. \tag{10}$$

As far as the solid-wall boundary conditions are concerned, the usual no-slip condition is prescribed for the velocity vector; since the vorticity conditions are of integral type (Quartapelle, 1993), the vorticity definition is used to evaluate its boundary values, for simplicity, as done by most researchers, see, e.g., Guj and Stella (1988); Orlandi (1987); Napolitano and Pascazio (1991); Guj and Stella (1993); Pascazio and Napolitano (1996); Lo, Murugesan, and Young (2005).

## 3 Numerical method

The vorticity transport equation and the velocity Poisson equation are written in Cartesian coordinates since only Cartesian grids are employed in this work. Indicating with $u_{(1)}$, $u_{(2)}$, $u_{(3)}$ ($u$, $v$, $w$) and $\omega_{(1)}$ $\omega_{(2)}$, $\omega_{(3)}$ the Cartesian components of $\vec{u}$ and $\vec{\omega}$ in the $x_{(1)}$, $x_{(2)}$, $x_{(3)}$ directions, respectively, the $i$-th component of the con-

servative vorticity transport equation (7) reads:

$$\frac{\partial \omega_{(i)}}{\partial t} - \frac{\partial \left[u_{(i)}\omega_{(j)} - u_{(j)}\omega_{(i)}\right]}{\partial x_{(j)}} - \frac{\partial \left[u_{(i)}\omega_{(k)} - u_{(k)}\omega_{(i)}\right]}{\partial x_{(k)}} = \frac{1}{Re}\left(\frac{\partial^2 \omega_{(i)}}{\partial x_{(i)}^2} + \frac{\partial^2 \omega_{(i)}}{\partial x_{(j)}^2} + \frac{\partial^2 \omega_{(i)}}{\partial x_{(k)}^2}\right), \tag{11}$$

where

$$j = (i+1) \mod 3, \qquad k = (i+2) \mod 3.$$

Using the non conservative equation (9), the left hand side of equation (11) reads:

$$\frac{\partial \omega_{(i)}}{\partial t} + u_{(i)}\frac{\partial \omega_{(i)}}{\partial x_{(i)}} + u_{(j)}\frac{\partial \omega_{(i)}}{\partial x_{(j)}} + u_{(k)}\frac{\partial \omega_{(i)}}{\partial x_{(k)}} - \omega_{(i)}\frac{\partial u_{(i)}}{\partial x_{(i)}} - \omega_{(j)}\frac{\partial u_{(i)}}{\partial x_{(j)}} - \omega_{(k)}\frac{\partial u_{(i)}}{\partial x_{(k)}}. \tag{12}$$

Finally, the $i$-th Cartesian component of the velocity-vector Poisson-equation (10) reads:

$$\frac{\partial^2 u_{(i)}}{\partial x_{(i)}^2} + \frac{\partial^2 u_{(i)}}{\partial x_{(j)}^2} + \frac{\partial^2 u_{(i)}}{\partial x_{(k)}^2} = \frac{\partial \omega_{(j)}}{\partial x_{(k)}} - \frac{\partial \omega_{(k)}}{\partial x_{(j)}}. \tag{13}$$

An implicit formulation is employed and the time derivative in the vorticity transport equation is discretized by a second-order-accurate three-level backward formula. Using a dual-time-stepping technique (Jameson, 1991), a pseudo-time derivative is introduced into the vorticity and velocity equations. Discretizing such derivatives with a two-level implicit Euler scheme and using the delta form of Beam and Warming (1978), the following semidiscrete equations for the incremental unknowns are obtained:

$$\frac{\Delta \omega_{(i)}}{\Delta \tau_\omega} + u_{(i)}\frac{\partial \Delta\omega_{(i)}}{\partial x_{(i)}} + u_{(j)}\frac{\partial \Delta\omega_{(i)}}{\partial x_{(j)}} + u_{(k)}\frac{\partial \Delta\omega_{(i)}}{\partial x_{(k)}} - \frac{\partial u_{(i)}}{\partial x_{(i)}}\Delta\omega_{(i)} = R_{(i)}, \tag{14}$$

$$\frac{\Delta u_{(i)}}{\Delta \tau_u} - \frac{\partial^2 \Delta u_{(i)}}{\partial x_{(i)}^2} - \frac{\partial^2 \Delta u_{(i)}}{\partial x_{(j)}^2} - \frac{\partial^2 \Delta u_{(i)}}{\partial x_{(k)}^2} = S_{(i)}. \tag{15}$$

In the equations above, $\Delta\tau_\omega$, $\Delta\tau_u$ are the pseudo-time steps, and $\Delta\omega_{(i)}$, $\Delta u_{(i)}$ are the unknowns, namely, the variations of the dependent variables at the new physical time level $(n+1)$ from the old pseudo-time level $(r)$ to the new one $(r+1)$; moreover, $R_{(i)}$ and $S_{(i)}$ indicate the right-hand-sides of the vorticity and velocity equations evaluated at $(n+1, r)$:

$$R_{(i)} = \frac{3\,\omega_{(i)}^{n+1,r} - 4\,\omega_{(i)}^{n} + \omega_{(i)}^{n-1}}{2\,\Delta t} + \left[\frac{\partial \left[u_{(i)}\omega_{(j)} - u_{(j)}\omega_{(i)}\right]}{\partial x_{(j)}} + \frac{\partial \left[u_{(i)}\omega_{(k)} - u_{(k)}\omega_{(i)}\right]}{\partial x_{(k)}} + \frac{1}{Re}\left(\frac{\partial^2 \omega_{(i)}}{\partial x_{(i)}^2} + \frac{\partial^2 \omega_{(i)}}{\partial x_{(j)}^2} + \frac{\partial^2 \omega_{(i)}}{\partial x_{(k)}^2}\right)\right]^{n+1,r}, \tag{16}$$

where $\Delta t$ is the physical time step, and

$$S_{(i)} = \left[\frac{\partial^2 u_{(i)}}{\partial x_{(i)}^2} + \frac{\partial^2 u_{(i)}}{\partial x_{(j)}^2} + \frac{\partial^2 u_{(i)}}{\partial x_{(k)}^2} - \frac{\partial \omega_{(j)}}{\partial x_{(k)}} + \frac{\partial \omega_{(k)}}{\partial x_{(j)}}\right]^{n+1,r}. \tag{17}$$

Note that in equations (14) and (15) only the corresponding variable is treated implicitly, leading to a decoupled system of equations. More importantly, equation (14) has been written according to a deferred correction approach (Khosla and Rubin, 1974), using the right-hand-side residual in the conservative form and the left-hand-side implicit operator in the non conservative one. In such a way, the converged solution at each physical time level enjoys the accuracy of the conservative second-order-accurate centred differences (Napolitano and Pascazio, 1991); moreover, employing upwind differences for the left-hand-side advection terms, the linear system is diagonally dominant, a favorable feature for any relaxation method.

An important feature of the present approach is the use of a staggered grid, which allows one to easily satisfy the discrete continuity equation and to obtain a divergence-free vorticity, see also Orlandi (1987); Napolitano and Pascazio (1991); Guj and Stella (1993); Bertagnolio and Daube (1997); Tenaud, Pellerin, Dulieu, and Phuoc (2005); Lo, Murugesan, and Young (2005). The staggered-grid arrangement of the variables is shown in figure 1: $\omega_{(1)}$ $\omega_{(2)}$, $\omega_{(3)}$ are evaluated at the centres of the edges parallel to the $x_{(1)}$, $x_{(2)}$, $x_{(3)}$ axes, respectively, whereas $u$, $v$, $w$ at the centres of the faces perpendicular to the same.

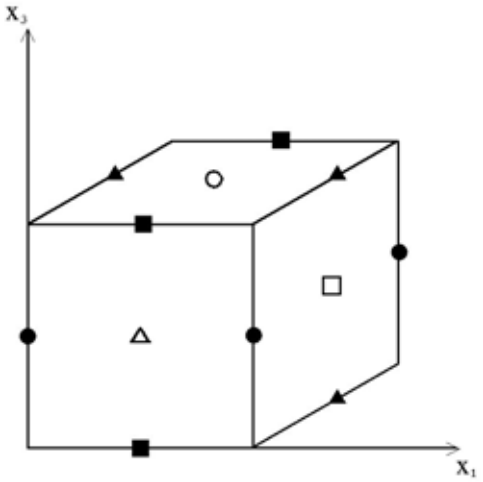


**Figure 1** : Three-dimensional staggered grid: ■ $\omega_{(1)}$, ▲ $\omega_{(2)}$, • $\omega_{(3)}$, □ $u$, △ $v$, ◯ $w$.

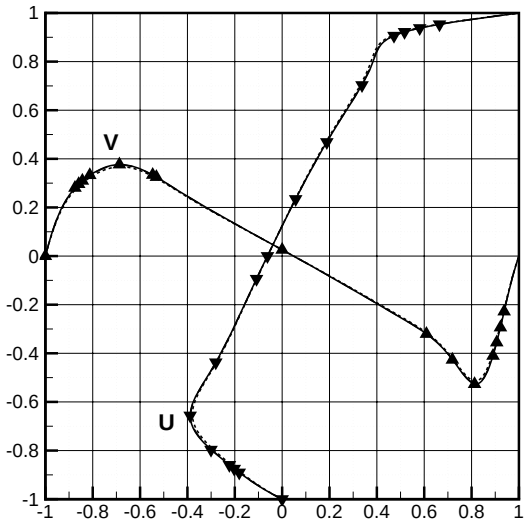


**Figure 2** : Mesh-refinement study for the two-dimensional driven cavity flow: velocity profiles; (- - - - -) $128^2$ cells; (– – –) $256^2$ cells; (———) $512^2$ cells; ▲, ▼ results of Botella and Peyret (1998).

The six uncoupled equations (14) and (15) are solved sequentially by a single application of one of the following relaxation schemes: forward-backward line-Gauss–Seidel combined with a three-level FAS multigrid scheme (Brandt, 1982) (LGS); the incomplete LU decomposition of Stone (1968) accelerated by a three-level FAS multigrid scheme (SIP); a stabilized conjugate gradient squared method with incomplete Cholesky preconditioning (CGS), see, e.g., Ferziger and Perić (1997); a combination of the SIP and CGS methods, obtained by performing sequentially the SIP and CGS schemes (SIP-CGS), has finally been introduced to achieve a more effective preconditioning of the CGS scheme. Concerning the multigrid strategy, full weighting collection and bilinear prolongation operators have been used (Napolitano and Pascazio, 1991). After driving the right-hand-side unsteady residuals to zero, the solution is advanced to the new physical time step. In all of the steady-flow computations $\Delta\tau_\omega = \Delta\tau_u = 1$; in unsteady ones, $\Delta\tau_u = 1$ whereas $\Delta\tau_\omega = 0.2\,\Delta t$, for stability; $\alpha = 0.92$ for the SIP solver in all but one computations; the CGS method is restarted every five iterations (or when convergence is reached).

In this paper, multi-block grids are used for the space discretization, which allow to handle multiply-connected domains and complex configurations and, more importantly, to solve each grid-block on a single processor of a parallel platform. In such an approach, the treatment of intra-block boundaries greatly affects the rate of convergence of the solution. A Schwarz additive algorithm with matching overlapping grids (Smith, Bjørstad, and Gropp, 1996) has been used and the influence on the convergence rate of the number of cells in the overlap region has been investigated.

All computations have been performed on an IBM eServer 1300 cluster of 16 dual Pentium III, 1.4 GHz, nodes.

## 4 Results

### *4.1 Two-dimensional flows*

The steady two-dimensional driven cavity problem at $Re = 1000$ has been solved as a test case to compare the performance of the various relaxation schemes. Numerical solutions have been obtained using three uniform Cartesian grids containing $128^2$, $256^2$ and $512^2$ cells. The $L^1$ norm of the largest residual has been reduced to $10^{-12}$ in all computations. Figures 2 and 3 provide the velocity profiles along the cavity centerlines and the vor-

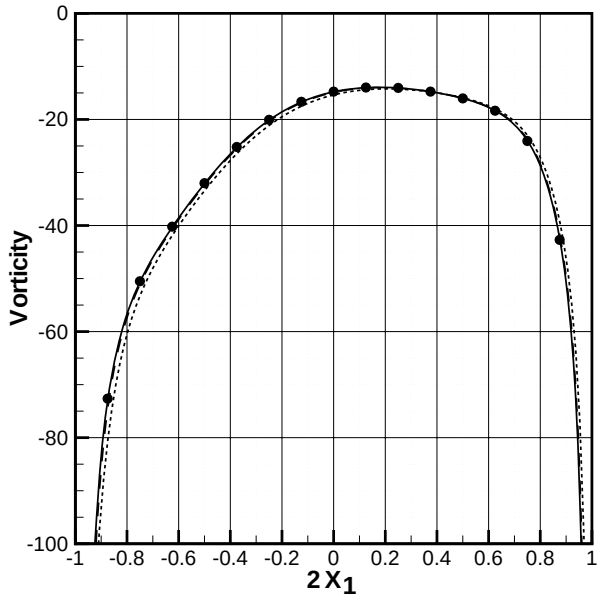


**Figure 3** : Mesh-refinement study for the two-dimensional driven cavity flow: vorticity distributions along the moving wall; (- - - - -) $128^2$ cells; (– – –) $256^2$ cells; (———) $512^2$ cells; ▲ results of Botella and Peyret (1998).

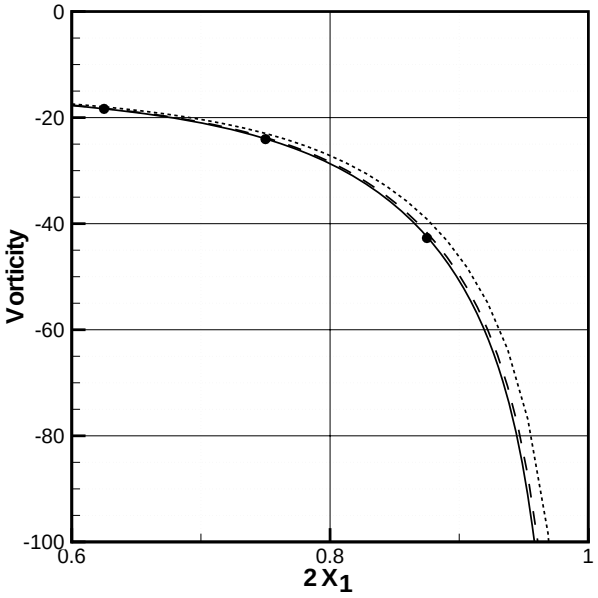


**Figure 5** : Mesh-refinement study for the two-dimensional driven cavity flow: blow-up of the vorticity distributions of figure 3.

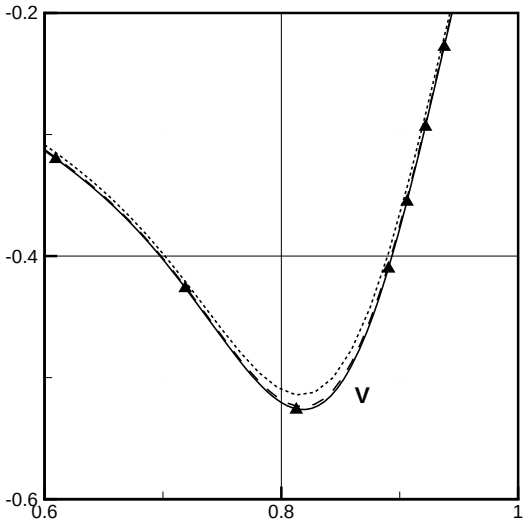


**Figure 4** : Mesh-refinement study for the two-dimensional driven cavity flow: blow-up of the velocity profiles of figure 2.

ticity along the moving wall, respectively. The results obtained with the two finer meshes are very close to each other, as seen in the blow-ups of figures 2 and 3, given in figures 4 and 5, and are in very good agreement with the benchmark results of Botella and Peyret (1998), also reported in figures 2-5.

The finest grid has been used to test the performance of the proposed parallel multi-block strategy. Tables 1 and 2 provide the number of iterations, $It$, and the computational times obtained with the four relaxation schemes when using a single block and 2, 4, and 9 equal-size blocks; for each multi-block computation, three different numbers of cells, $N_c$, in the overlap region have been considered. The tables provide also the speed-ups, $S$, namely, the ratio between the CPU times of the single-block computation and of the multi-block one. It appears that the efficiency increases going from the LGS method to the SIP-CGS one and, more importantly, that the modification of the preconditioning procedure by means of the SIP method is indeed effective. Concerning the performance of the multi-block parallel procedure, the number of cells in the overlap region plays a fundamental role,

**Table 1** : Parallel efficiency: computational time for the 2D driven cavity flow using LGS and SIP.

| | Blks | $N_c$ | *It* | CPU $[s]$ | *S* |
|---|---|---|---|---|---|
| LGS | 1 | – | 23803 | 156686 | – |
| | 2 | 1 | 26072 | 85476 | 1.83 |
| | | 5 | 24320 | 79695 | 1.97 |
| | | 9 | 24245 | 79576 | 1.97 |
| | 4 | 1 | 29885 | 51255 | 3.06 |
| | | 5 | 27872 | 42537 | 3.69 |
| | | 9 | 26710 | 41761 | 3.75 |
| | 9 | 1 | 33408 | 24750 | 6.33 |
| | | 9 | 26898 | 21371 | 7.33 |
| | | 17 | 24623 | 19733 | 7.94 |
| SIP | 1 | – | 7349 | 28775 | – |
| | 2 | 1 | 8423 | 15492 | 1.86 |
| | | 5 | 7382 | 14464 | 1.99 |
| | | 9 | 7352 | 14417 | 2.00 |
| | 4 | 1 | 10857 | 10365 | 2.78 |
| | | 5 | 7630 | 7274 | 3.96 |
| | | 9 | 7374 | 7206 | 3.99 |
| | 9 | 1 | 11473 | 4967 | 5.79 |
| | | 9 | 8528 | 3813 | 7.55 |
| | | 17 | 7519 | 3309 | 8.70 |

**Table 2** : Parallel efficiency: computational time for the 2D driven cavity flow using CGS and SIP-CGS.

| | Blks | $N_c$ | *It* | CPU $[s]$ | *S* |
|---|---|---|---|---|---|
| CGS | 1 | – | 3867 | 21475 | – |
| | 2 | 1 | 8427 | 23594 | 0.91 |
| | | 5 | 5328 | 14500 | 1.48 |
| | | 9 | 4410 | 13153 | 1.63 |
| | 4 | 1 | 13573 | 21174 | 1.01 |
| | | 5 | 6822 | 10188 | 2.11 |
| | | 9 | 4474 | 6685 | 3.21 |
| | 9 | 1 | 11812 | 7263 | 2.96 |
| | | 9 | 6969 | 4321 | 4.97 |
| | | 17 | 5735 | 3602 | 5.96 |
| SIP-CGS | 1 | – | 1827 | 11143 | – |
| | 2 | 1 | 4110 | 11960 | 0.93 |
| | | 5 | 2319 | 7119 | 1.57 |
| | | 9 | 2008 | 6180 | 1.80 |
| | 4 | 1 | 5245 | 8441 | 1.32 |
| | | 5 | 2782 | 4322 | 2.58 |
| | | 9 | 2699 | 4275 | 2.61 |
| | 9 | 1 | 5697 | 3857 | 2.89 |
| | | 9 | 3619 | 2415 | 4.61 |
| | | 17 | 3377 | 2265 | 4.92 |

the speed-up increasing with the number of such cells. In particular, for the nine-block case, the CPU times of the LGS and SIP methods scale linearly with the number of processors if one uses 17 cells in the overlap region. On the other hand, the *more implicit* CGS and SIP-CGS methods do not achieve the theoretical linear scaling, indicating that for such relaxation schemes the present multi-block strategy associated with the decoupled implicit approach is not fully satisfactory. Therefore, only the LGS and SIP methods have been used in the three-dimensional flow simulations.

Then, the unsteady flow past a square cylinder at $Re = 150$ has been computed using the SIP-CGS method; the mesh with eight blocks and $168 \times 120$ cells employed by Sohankar, Norberg, and Davidson (1999), see figure 6, as well as a finer grid with a total of $336 \times 240$ cells have been used, with $\Delta t = 0.025$ and $\Delta t = 0.0125$, respectively. The uniform velocity has been imposed at the far-field left, upper and lower boundaries, whereas the velocity at the right (outlet) far-field boundary has been linearly extrapolated from the two neighbouring left points. Obviously, the (scalar) vorticity at all boundary points has been computed by its definition, namely, the $x_{(3)}$ component of equation (3). At each time step, the $L^1$ norm of the largest unsteady residual has been reduced to $10^{-7}$, within about 350 iterations (about 40 CPU seconds) on the coarser grid. Figures 7 and 8 provide the horizontal and vertical velocity components at $x_{(2)} = 0$ and $x_{(1)} = 4$ and 7, respectively, the origin of the Cartesian axes coinciding with the centre of the square. The finer-grid results are shown as symbols and clearly indicate grid convergence. On both grids the computed Strouhal number is equal to 0.165, which corresponds to the value provided by Sohankar, Norberg, and Davidson (1999).

### *4.2 Three-dimensional flows*

The parallel performance of the three-dimensional implementation of the proposed approach, using the LGS and SIP methods, has been tested versus the steady flow in a cubic cavity at $Re = 100$; the top wall perpendicular to the $x_{(3)}$ axis moves along the $x_{(1)}$ direction. A uniform Cartesian grid with $64^3$ cells has been used and the $L^1$ norm of the largest residual has been re-

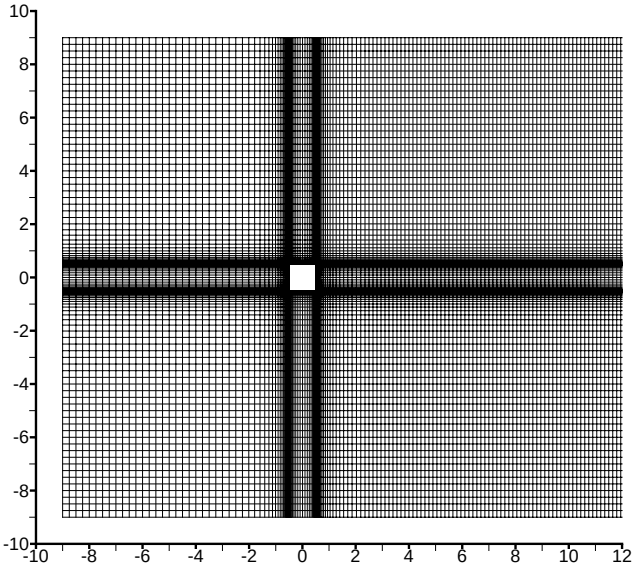

**Figure 6** : Flow past a square cylinder: Computational grid.

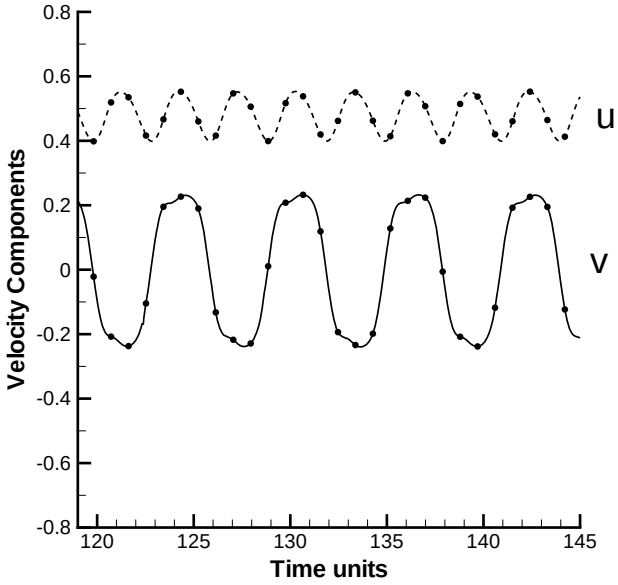


**Figure 7** : Flow past a square cylinder: time history of the velocity components at $x_{(1)} = 4$ and $x_{(2)} = 0$.

duced to $10^{-12}$. For both methods, a three-level multi-grid scheme has been employed and for the SIP method

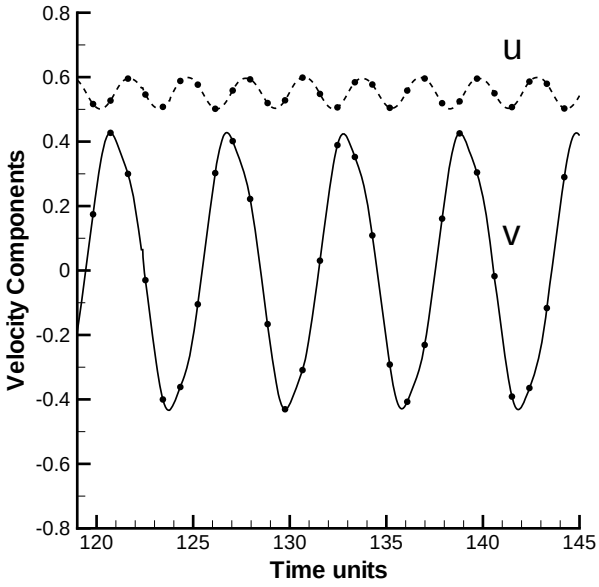


**Figure 8** : Flow past a square cylinder: time history of the velocity components at $x_{(1)} = 7$ and $x_{(2)} = 0$.

**Table 3** : Parallel efficiency: computational time for the 3D driven cavity flow.

| | Blks | $N_c$ | *It* | CPU $[s]$ | *S* |
|---|---|---|---|---|---|
| LGS | 1 | – | 234 | 4105 | – |
| | 2 | 1 | 476 | 4162 | 0.99 |
| | | 5 | 248 | 2173 | 1.89 |
| | | 9 | 213 | 1861 | 2.21 |
| | 4 | 1 | 953 | 4116 | 1.00 |
| | | 5 | 433 | 1878 | 2.19 |
| | | 9 | 294 | 1271 | 3.23 |
| | 8 | 1 | 1336 | 2837 | 1.45 |
| | | 5 | 566 | 1195 | 3.44 |
| | | 9 | 350 | 742 | 5.53 |
| SIP | 1 | – | 202 | 1448 | – |
| | 2 | 1 | 442 | 1601 | 0.90 |
| | | 5 | 182 | 661 | 2.19 |
| | | 9 | 167 | 603 | 2.40 |
| | 4 | 1 | 933 | 1701 | 0.85 |
| | | 5 | 298 | 548 | 2.64 |
| | | 9 | 203 | 370 | 3.91 |
| | 8 | 1 | 1410 | 1285 | 1.13 |
| | | 5 | 380 | 345 | 4.19 |
| | | 9 | 257 | 241 | 6.01 |

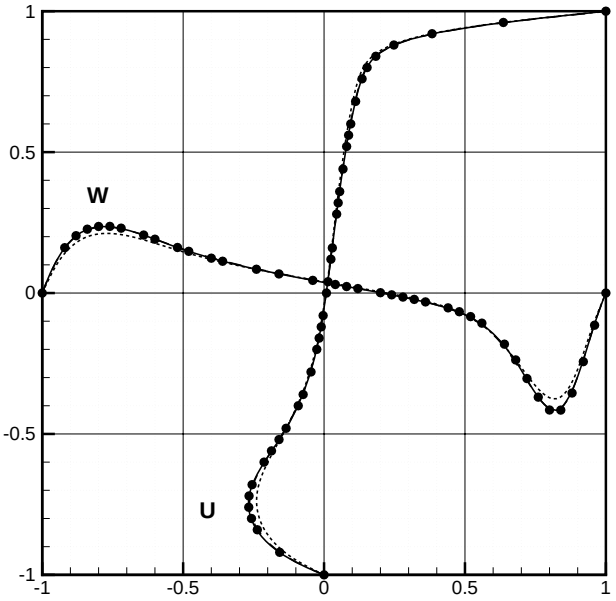


**Figure 9** : Mesh-refinement study for the three-dimensional driven cavity flow at $Re = 1000$: (- - - -) $40^3$ cells; (– – –) $64^3$ cells; (——) $80^3$ cells; • numerical results of Lo, Murugesan, and Young (2005).

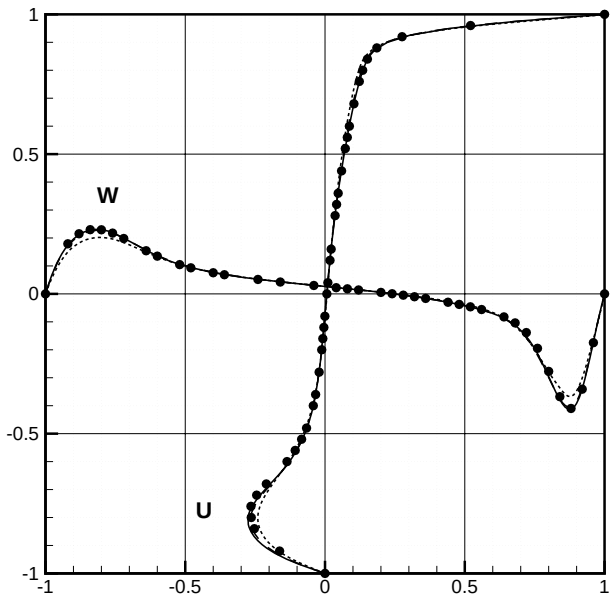


**Figure 10** : Mesh-refinement study for the three-dimensional driven cavity flow at $Re = 2000$: (- - - -) $40^3$ cells; (– – –) $64^3$ cells; (——) $80^3$ cells; • numerical results of Lo, Murugesan, and Young (2005).

$\alpha$ was set equal to 0.9. Table 3 provides the number of iterations and the computational times obtained with the two relaxation schemes when using a single block and 2, 4, and 8 equal-size blocks, as well as the corresponding speed-ups; again, for each multi-block computation, three different numbers of cells in the overlap region have been used. Concerning the performance of the multi-block parallel procedure, the speed-up of the more efficient SIP method is almost linear when using 9 cells in the overlap region and, again, is higher than that provided by the LGS method. With respect to the two-dimensional case, a slight decrease of the speed-up is observed, as expected; a greater number of cells in the overlap region is thus needed to approach the theoretical linear scaling. Moreover, the parallel performance of the three-dimensional approach is inferior to that of the two-dimensional one, mainly for the increased communication between neighboring processors.

In order to verify the accuracy of the proposed method, the cubical lid-driven cavity flow problem has been computed for Reynolds number equal to 1000, 2000 and 3200. Stretched grids containing $40^3$, $64^3$, and $80^3$ cells have been used:

$$x_{(1)} = \frac{1}{2} + \frac{1}{2}\frac{\tanh\left[a\frac{i-i_{mid}}{(i_{mid}-1)}\right]}{\tanh a}, \tag{18}$$

$$x_{(2)} = \frac{1}{2} + \frac{1}{2}\frac{\tanh\left[a\frac{j-j_{mid}}{(j_{mid}-1)}\right]}{\tanh a}, \tag{19}$$

$$x_{(3)} = \frac{1}{2} + \frac{1}{2}\frac{\tanh\left[a\frac{k-k_{mid}}{(k_{mid}-1)}\right]}{\tanh a}, \tag{20}$$

the constant $a$ being equal to 1.1 and $i_{mid} = j_{mid} = k_{mid} =$ 21, 33, and 41 for the three grids.

In the cubical lid-driven cavity, the mid-plane along the $x_{(2)}$ direction is the plane of symmetry when the flow is steady, $Re = 1000$ and 2000. At $Re = 3200$ the flow becomes unsteady and the symmetry is lost for the instantaneous quantities.

For $Re = 1000$ and $Re = 2000$, figures 9 and 10 show the $u$ and $w$ profiles along the centerlines $(x_{(1)} = x_{(2)} = 1/2)$ and $(x_{(2)} = x_{(3)} = 1/2)$ for $Re = 1000$ and 2000, respectively. Both figures provide the results obtained by the present approach using the three aforementioned grids, together with the results of Lo, Murugesan, and Young

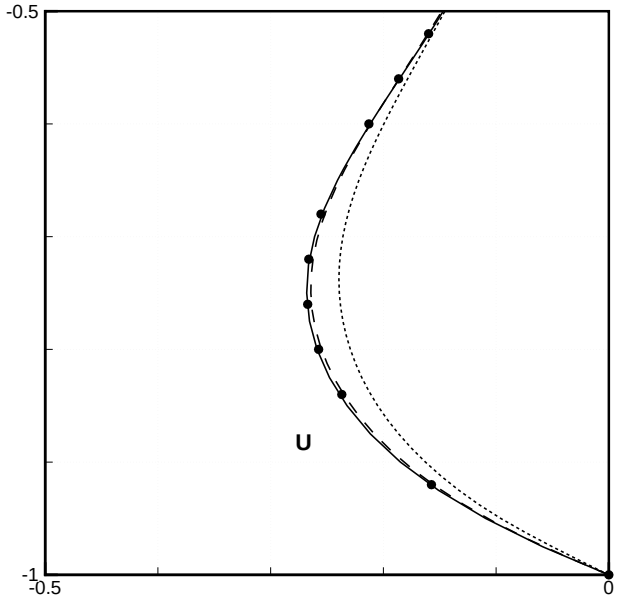


**Figure 11** : Blow-up of the velocity profiles of figure 9.

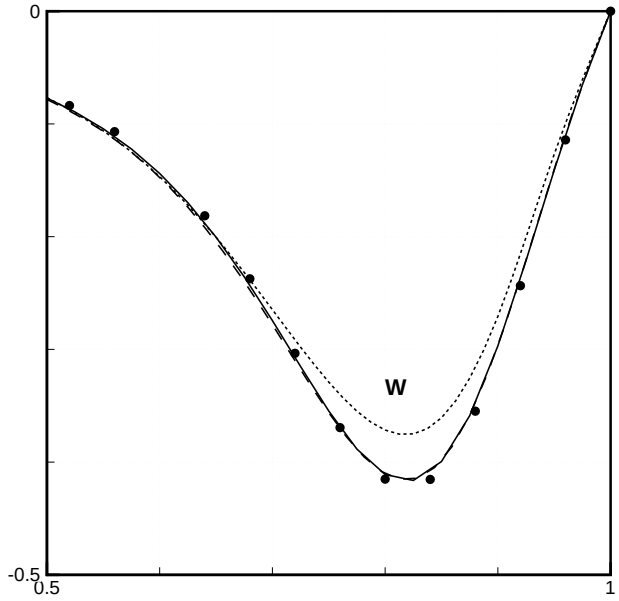


**Figure 12** : Blow-up of the velocity profiles of figure 9.

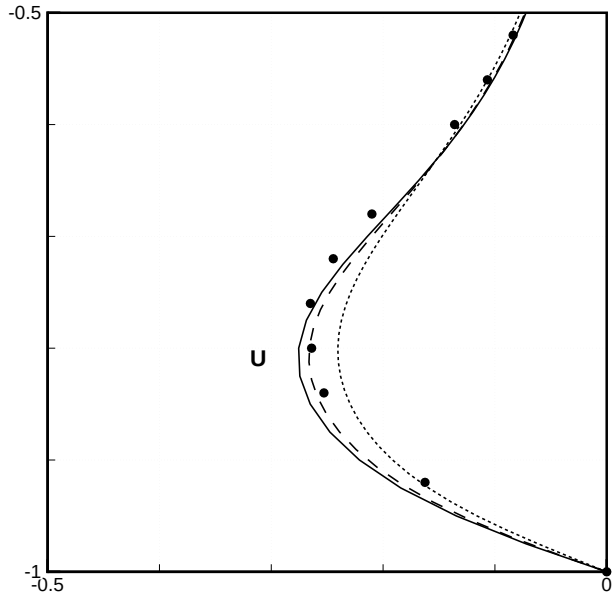


**Figure 13** : Blow-up of the velocity profiles of figure 10.

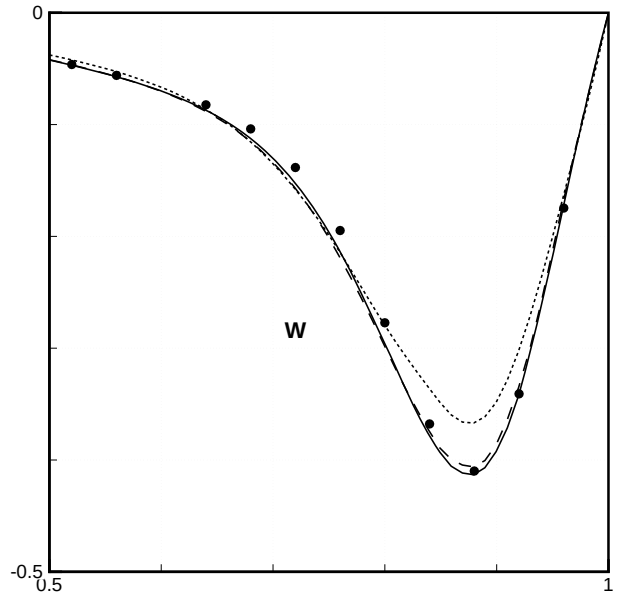


**Figure 14** : Blow-up of the velocity profiles of figure 10.

(2005), using a uniform Cartesian grid with $80^3$ cells, the agreement is quite good. More importantly, the finest-grid present solutions can be considered to be grid-converged, see figures 11-14, which provide blow-ups of the velocity profiles of figures 9 and 10. The accuracy of the solutions is further demonstrated by the perfect symmetry of the vertical flow (about $x_{(2)}$) obtained for both $Re = 1000$ and $Re = 2000$, see figures 15 and 16, which provide the contour lines of $\omega_{(3)}$ in the $x_{(1)} - x_{(2)}$ plane at $x_{(3)} = 1/2$.

For $Re = 3200$, the flow is unsteady and the detailed experimental data of Prasad and Koseff (1989) as well as

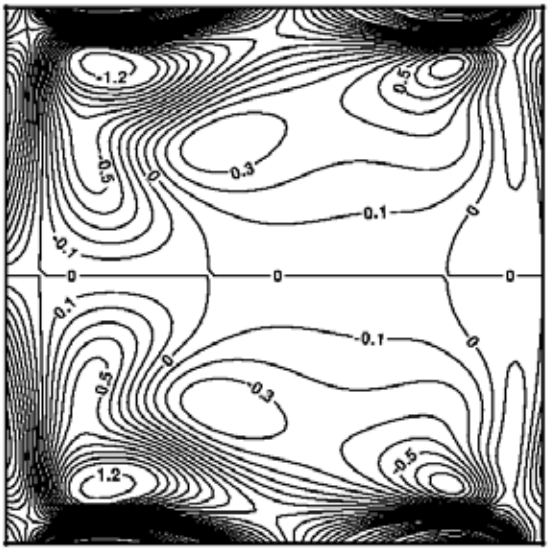


**Figure 15** : Contour lines of the $x_{(3)}$ vorticity component at $x_{(3)} = 1/2$ plane for $Re = 1000$

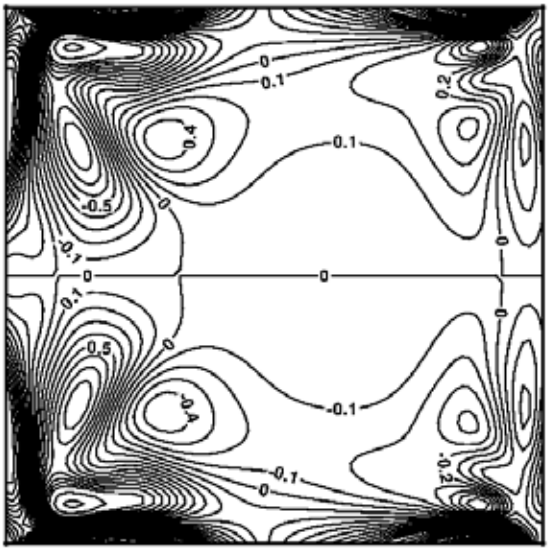


**Figure 16** : Contour lines of the $x_{(3)}$ vorticity component at $x_{(3)} = 1/2$ plane for $Re = 2000$

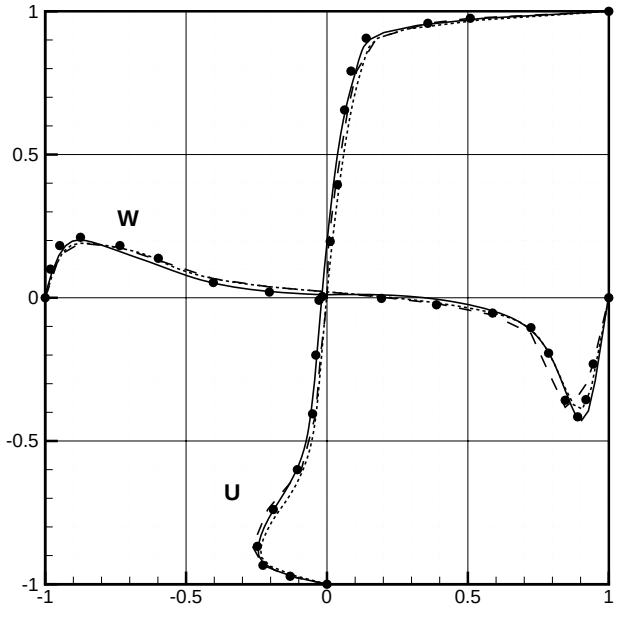


**Figure 17** : Mean velocity profiles for $Re = 3200$: (——) present results, $80^3$ cells; (- - - - -) present results, $64^3$ cells; (– – – –) numerical results of Deshpande and Milton (1998); • experimental results of Prasad and Koseff (1989).

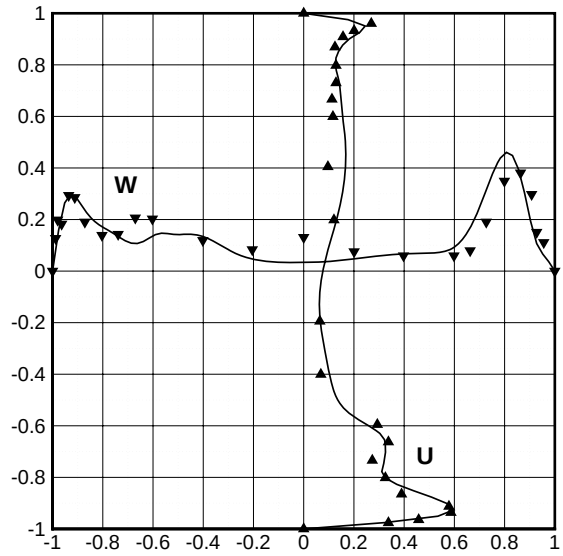


**Figure 18** : $10 \times rms$ of the fluctuating velocity at $Re = 3200$: (——) present results, $80^3$ cells; ▲, ▼ experimental data of Prasad and Koseff (1989).

the numerical results of Deshpande and Milton (1998) are used to assess the capability of the proposed unsteady solver. Numerical results have been obtained using the above mentioned meshes with $64^3$ and $80^3$ cells and a

time step equal to $\Delta t = 0.05$. At each time step, the $L^1$ norm of the largest unsteady residual has been reduced to $10^{-7}$ by about 300 SIP iterations, corresponding to about 370 CPU seconds on the aforementioned computer, using the finest mesh and 16 blocks. Figures 17 and 18 provide the mean velocity profiles and the corresponding *rms* fluctuations along the cavity centerlines at $x_{(2)} = 1/2$. It appears that the present finer-grid solutions are in very good agreement with both the reference numerical ones and the experimental data.

## 5 Conclusions

An efficient and accurate numerical method for solving unsteady incompressible flows has been presented. The method employs the vorticity-velocity formulation of the Navier–Stokes equations, the vorticity transport equation being coupled with a Poisson equation for the velocity vector. The equations are discretized in space by staggered-grid second-order-accurate finite-differences and the vorticity transport equation is discretized in time by means of an implicit three-level scheme. Each equation is supplemented with a pseudo-time derivative, in order to employ different efficient relaxation schemes to converge the solution at each physical time level. Steady flows are computed by dropping the physical time derivative and converging the pseudo-time-dependent problem. A domain decomposition of the physical space is also employed, which allows one to handle multiply-connected domains and complex configurations and, more importantly, to solve each grid-block on a single processor of a parallel platform. The Schwarz additive algorithm with matching overlapping grids, used for the intra-block boundary treatment in parallel computations, has been effective in conjunction with either a line-Gauss–Seidel or a strongly implicit procedure, both accelerated by a multigrid scheme. The accuracy and efficiency of the proposed methodology has been verified by solving well known two-dimensional flow problems as well as the three-dimensional steady and unsteady flows inside a cubic cavity.

**Acknowledgement:** This research has been supported by MIUR, grants Cofinlab2000 and Cofin2003.

## References

**Beam, R. M.; Warming, R. F.** (1978): An implicit factored scheme for the compressible Navier-Stokes equations. *AIAA J.*, vol. 16, pp. 393–402.

**Bertagnolio, F.; Daube, O.** (1997): Solution of the div-curl problem in generalized curvilinear coordinates. *J. Comput. Phys.*, vol. 138, pp. 121–152.

**Botella, O.; Peyret, R.** (1998): Benchmark spectral results of the lid-driven cavity flow. *Comput. Fluids*, vol. 27, pp. 421–433.

**Brandt, A.** (1982): Guide to multigrid development. *Lecture Notes in Mathematics*, vol. 960, pp. 220–312.

**De Palma, P.; Pascazio, G.; Napolitano, M.** (2001): Accurate and efficient solutions of unsteady viscous flows. *Int. J. Num. Meth. Heat and Fluid Flow*, vol. 11, pp. 286–307.

**Deshpande, M.; Milton, S. G.** (1998): Kolmogorov scales in a driven cavity flow. *Fluid Dynamics Research*, vol. 22, pp. 359–381.

**Fasel, H.** (1976): Investigation of the stability of bouondary-layers by a finite-difference model of the Navier-Stokes equations. *J. Fluid Mech.*, vol. 78, pp. 355–383.

**Ferziger, J. H.; Perić, M.** (1997): *Computational methods for fluid dynamics*. Springer Verlag, Berlin Heidelberg.

**Guj, G.; Stella, F.** (1988): Numerical solutions of the high-Re recirculating flows in vorticity-velocity form. *Int. J. Numer. Meth. Fluids*, vol. 8, pp. 405–416.

**Guj, G.; Stella, F.** (1993): A vorticity-velocity method for the numerical solution of 3D incompressible flows. *J. Comput. Phys.*, vol. 106, pp. 286–298.

**Jameson, A.** (1991): Time dependent calculations using multigrid with applications to unsteady flows past airfoils and wings. Technical report, AIAA Paper 91–1596, 1991.

**Khosla, P. K.; Rubin, S. G.** (1974): A diagonally dominant second-order-accurate implicit scheme. *Comput. Fluids*, vol. 2, pp. 207–209.

**Lo, D. C.; Murugesan, K.; Young, D. L.** (2005): Numerical solution of three-dimensional velocity-vorticity Navier–Stokes equations by finite difference method. *Int. J. Numer. Meth. Fluids*, vol. 47, pp. 1469–1487.

**Mansfield, J. R.; Knio, O. M.; Menevau, C.** (1998): A dynamic les scheme for the vorticity transport equation: formulation and *a priori* tests. *J. Comput. Phys.*, vol. 145, pp. 693–730.

**Napolitano, M.; Pascazio, G.** (1991): A numerical method for the vorticity-velocity navier-stokes equations in two and three dimensions. *Comput. Fluids*, vol. 19, pp. 489–495.

**Orlandi, P.** (1987): Vorticity-velocity formulation for high re flows. *Comput. Fluids*, vol. 15, pp. 137–149.

**Pascazio, G.; Grimaldi, A.; Napolitano, M.** (2003): An accurate and efficient technique for unsteady viscous flows in two dimensions. In S. Armfield, P. Morgan, K. S.(Ed): *Computational Fluid Dynamics 2002*, pp. 725–730, New York. Springer.

**Pascazio, G.; Napolitano, M.** (1996): A staggered-grid finite volume method for the vorticity-velocity equations. *Comput. Fluids*, vol. 25, pp. 433–446.

**Prasad, A. K.; Koseff, J. R.** (1989): Reynolds number and end-wall effects on a lid-driven cavity flow. *Phys. Fluids*, vol. 1, pp. 208–218.

**Quartapelle, L.** (1993): *Numerical solution of incompressible Navier–Stokes equations*. Birkhauser, Basel.

**Smith, B.; Bjørstad, P.; Gropp, W.** (1996): *Domain decomposition: parallel multilevel methods for elliptic partial differential equations*. Cambridge University Press, Cambridge.

**Sohankar, A.; Norberg, C.; Davidson, L.** (1999): Simulation of three-dimensional flow around a square cylinder at moderate reynolds numbers. *Phys. Fluids*, vol. 11, pp. 288–306.

**Speziale, C. G.** (1987): On the advantages of the vorticity-velocity formulation of the Navier–Stokes equations of fluid dynamics. *J. Comput. Phys.*, vol. 73, pp. 476–480.

**Stone, H.** (1968): Iterative solution of implicit approximations of multidimentional partial differential equations. *SIAM J. Numer. Anal.*, vol. 5, pp. 530.

**Tenaud, C.; Pellerin, S.; Dulieu, A.; Phuoc, L. T.** (2005): Large eddy simulations of a spatially developing incompressible 3D mixing layer using the $\mathbf{v} - \omega$ formulation. *Comput. Fluids*, vol. 34, pp. 67–96.

**Winckelmans, G. S.; Lund, T. S.; Carati, D.; Wray, A. A.** (1996): A priori testing of subgrid-scale models for the velocity-pressure and vorticity-velocity formulations. In Center for Turbulence Research, S. U.(Ed): *Proceedings of the Summer Program,*, pp. 309–328.